Article

The Influence of La and Ce Addition on Inclusion Modification in Cast Niobium Microalloyed Steels

Hadi Torkamani [1,*], Shahram Raygan [1,*], Carlos Garcia Mateo [2,*] [ID], Jafar Rassizadehghani [1], Javier Vivas [2], Yahya Palizdar [3] and David San-Martin [2]

[1] School of Metallurgy and Materials Engineering, College of Engineering, University of Tehran, 111554563 Tehran, Iran; jghani@ut.ac.ir
[2] Materalia Research Group, National Center for Metallurgical Research (CENIM), Consejo Superior de Investigaciones Científicas (CSIC), E–28040 Madrid, Spain; jvm@cenim.csic.es (J.V.); dsm@cenim.csic.es (D.S.-M.)
[3] Research Department of Nano-Technology and Advanced Materials, Materials and Energy Research Center, 3177983634 Karaj, Iran; y.palizdar@merc.ac.ir
[*] Correspondence: h.torkamani@ut.ac.ir (H.T.); shraygan@ut.ac.ir (S.R.); cgm@cenim.csic.es (C.G.M.), Tel.: +98-912-221-3206 (H.T.); +98-218-801-2999 (S.R.); +34-91-553-8900 (C.G.M)

Abstract: The main role of Rare Earth (RE) elements in the steelmaking industry is to affect the nature of inclusions (composition, geometry, size and volume fraction), which can potentially lead to the improvement of some mechanical properties such as the toughness in steels. In this study, different amounts of RE were added to a niobium microalloyed steel in as-cast condition to investigate its influence on: (i) type of inclusions and (ii) precipitation of niobium carbides. The characterization of the microstructure by optical, scanning and transmission electron microscopy shows that: (1) the addition of RE elements change the inclusion formation route during solidification; RE > 200 ppm promote formation of complex inclusions with a $(La,Ce)(S,O)$ matrix instead of Al_2O_3-MnS inclusions; (2) the roundness of inclusions increases with RE, whereas more than 200 ppm addition would increase the area fraction and size of the inclusions; (3) it was found that the presence of MnS in the base and low RE-added steel provide nucleation sites for the precipitation of coarse niobium carbides and/or carbonitrides at the matrix–MnS interface. Thermodynamic calculations show that temperatures of the order of 1200 °C would be necessary to dissolve these coarse Nb-rich carbides so as to reprecipitate them as nanoparticles in the matrix.

Keywords: niobium microalloyed steel; as-cast condition; inclusion; rare earth elements; precipitation

1. Introduction

The chemical composition, population density, and morphology of non-metallic inclusions in metals are among the key factors determining the steels' quality [1–4]. These issues have become the leading subjects in the field of steelmaking processes in the last few decades.

Rare Earth (RE) elements are known as non-metallic inclusion modifiers that can be added into the molten steel in the form of misch metal, a master alloy consisting of rare earth elements such as Ce and La. In contrast to MnS, RE-based inclusions do not deform during hot metal working i.e., they keep their spherical shape, which seems to be more beneficial for the toughness. In fact, despite various roles of RE in steels, the main use of RE in steels concerns the shape control of inclusions, especially MnS particles during the hot deformation processes [5–9]. It has been suggested that the addition of these elements results in a considerable change in inclusion composition and generally leads to the formation of several constituents such as oxysulphides (Ce_2O_2S, La_2O_2S), oxides (Ce_2O_3, La_2O_3) and sulfides (Ce_2S_3, La_2S_3) [10,11].

The standard Gibbs free energy (ΔG°) for the formation of characteristic La- and Ce-based oxides/sulfides is given in Table 1. The values contained in this table have been obtained from different references [12–14]. From this table, it can be discovered that at high temperatures, this energy is so negative that it causes the formation of these components right after their addition into the liquid steel; however, due to their densities, the removal of the RE inclusions from the molten steel is relatively difficult [7,10,11,15–17]. Table 2 illustrates the melting point and density of some typical La and Ce oxides and sulfides. The values shown in this table have been taken from Ref. [11].

Table 1. Standard Gibbs energy (ΔG°= A + BT) of the formation of oxide and sulfide of La and Ce and its value at 1600 °C (1873 K) [12–14].

Compound	A, J mol^{-1}	B, J (mol K)$^{-1}$	$\Delta G^\circ_{1873\ K}$ kJ mol^{-1}
Ce_2O_3	-1.30×10^6	374	-600
La_2O_3	-1.44×10^6	337	-810
Ce_2S_3	-1.02×10^6	340	-383
La_2S_3	-1.27×10^6	417	-490

Table 2. Physical properties of oxide and sulfide of La and Ce [11].

Compound	Melting Point °C	Density kg/m^3
Ce_2O_3	~2177	6200
La_2O_3	~2249	6500
Ce_2S_3	~2150	5020
La_2S_3	~2099	5000

Although the effects of RE on the shape, fraction and distribution of inclusions have been widely studied, it seems that there is no unanimity in this regard. For instance, Grajcar et al. [9] suggested that the area fraction of non-metallic inclusions in the steels modified by misch metal was in the range of 0.0012 to 0.0018, which was twice as low as that of untreated steels, while the average area of the particles was the same for both conditions. On the other hand, Handerhan et al. [18] reported that the volume fraction of inclusions has been similar for the base and RE-added steels, but inclusions in the samples with RE were larger, which led to a larger interspacing of the inclusions. The same result was also reported elsewhere [15]. In contrast, Belyakova et al. [19] suggested that the number of inclusions increased by RE addition. In another work, it has been shown that when 0.35 kg/ton of misch metal is added to the molten steel, it results in obtaining a higher volume fraction of inclusions compared to the untreated steel [10]. However, adding higher amounts of RE could change the size distribution of the inclusions. In addition, it has been observed that the size of the inclusions decreases with low level of RE addition while it increases with higher level of RE addition; this somehow implies that the optimum amount of RE should be added to the steel [5].

The reasons for obtaining these different results (sometimes contradictory) could be attributed to the different steel making processes used in the various studies. For example, longer holding time during the ladle treatment after RE addition would cause more deposition or floatation of the inclusions. The location in the casting where the investigated samples have been taken can be another reason for such disagreements. Regarding the latter case, Paul et al. [10] studied the distribution and composition of the different inclusions in RE treated steels and showed that there is a considerable difference between the bottom and top of the ingots.

On the other hand, having reviewed the literature, there has been a large number of investigations pertaining to the use of RE elements through the hot deformation processes to derive benefits from the size and shape control of the inclusions at that stage. However, the contribution of as-cast condition to the inclusion characterization and consequently to the obtained properties has not been completely disclosed. In fact, there is little recent information in the literature concerned with the inclusion modification effects due to RE addition in cast steels while both steelmaking practice and steel compositions have considerably changed over the past decades.

Moreover, few studies have reported that the RE addition could improve the solubility of Nb and consequently nanoprecipitation behavior in steels, but there is no certain consensus about its mechanism [20,21].

In this work, an Nb-containing microalloyed steel has been selected to investigate the effects of RE addition on the modification of non-metallic inclusions as well as on the nanoprecipitation behavior in the as-cast condition. As it is discussed in the next sections, the results allow us to clarify the effects of RE addition (amount) on inclusion characteristics (size and composition) and also on the nanoprecipitation of Nb- and V-carbonitrides, which is directly related to the nature of inclusions formed in each alloy.

2. Experimental Procedure

2.1. Casting and History of Samples

Clean scrap steel was melted in a 100 kg capacity induction furnace under the air atmosphere. Once the melt reached to 1650 °C, the amounts of alloying elements were adjusted and the chemical composition was measured by using the Optical Emission Spectrometry (OES) technique on site. Since rare earth elements are strong oxide forming elements, it is desirable to add misch metal to the molten steel when the oxygen level is as low as possible. In order to meet this requirement, aluminum was added as deoxidizer to the melt prior to pouring the melt into the carrying ladle and adding the RE.

Three different amounts (2.5, 7 and 9 gr) of misch metal, containing 37.8 wt. % La and 62.1 wt. % Ce, were placed at the bottom of the 25 kg capacity carrying ladle as the last addition. In fact, the same melt with a base composition (Table 3) was used for all the castings while different amounts of RE were added to the melts to ensure obtaining the same compositions as the base steel but with different amounts of RE. The loss of RE elements in steelmaking is remarkably practice-dependent while many conducted studies only reported the amount of added rare earth elements per kg of molten steel. Hereupon, the amounts of RE in the ingots were measured by the Inductively Coupled Plasma (ICP) technique, the results of which are given in Table 4. In addition, the amount of O and N in the ingots was measured by using a gas analyzing equipment (model: LECO TC-436 AR (LECO Corporation, Saint Joseph, MI, USA) for the studied steels; the results are shown in Table 4. Regarding the amount of sulfur in these steels, it did not change compared to that of the base steel (Table 3). This result seems reasonable because the misch metal was added to the ladle after deoxidation and removal of floated impurities (steel slag); thus, RE would not have a considerable effect on the S content and this element would place in solid solution as well as forming the sulfide particles distributed through the as-cast ingot.

The ingots experienced homogenization treatment at 1100 °C for 5 h, and then smaller test samples were normalized at 950 °C for 30 min prior to their inspection under the microscopes.

Table 3. Chemical composition of the base microalloyed steel (Fe to balance).

Elements	C	Si	Mn	S	P	V	Nb	Mo	Cu	Al	Cr
wt. %	0.16	0.30	1.00	0.01	0.02	0.11	0.05	0.01	0.09	0.04	0.06

Table 4. Amounts of rare earth (RE) elements (La and Ce), O and N in different samples.

Steels	Elements, ppm				
	Ce	*La*	*Ce + La*	*O*	*N*
RE1	<10	<10	—	96 ± 10	113 ± 4
RE2	37.5	17.5	55.0	116 ± 35	114 ± 3
RE3	127.0	72.5	199.5	93 ± 6	112 ± 3
RE4	192.0	100.0	292.0	110 ± 14	114 ± 1

2.2. Sample Preparation and Metallographic Observations

Prior to inspection by Optical Microscopy (OM), the steel samples were ground and polished using standard metallographic procedures. Inclusion characterizations are usually carried out on optical micrographs taken from the polished surface to achieve better contrasts between the inclusions and the matrix. Therefore, the microstructure was characterized in the as-polished condition. Since the surface of the samples might react with water, the samples were dryly ground. In addition, special care was taken during grinding and polishing; controlled force was exerted on the samples during grinding to prevent removal of inclusions from the surface. In addition, a lubricant, which was a mix of ethanol and DP-Lubricant Blue (DP stands for Diamond Polishing; Struers Aps, Ballerup, Denmark), was used for polishing to ensure prevention of oxidation or any possible errors committed through the assessment of inclusions. In the last step of this preparation, ethanol was also used to remove any products coming from the polishing steps. The characterization of the area fraction, average area and roundness factor of the inclusions was carried out with the aid of an image analyzing program (Image J 1.47v, free software developed at the National Institute of Mental Health (NIMH), Bethesda, MD, USA) on at least five random micrographs using the same magnification for all the steel samples. For this characterization, the samples were extracted from the middle and 3 cm from the bottom of each Y block ingots (Figure 1). Considering the inclusions as circular in 2D, the average size (d) was calculated from their average area (A) according to $d = 2 \sqrt{(A/\pi)}$.

Scanning Electron Microscopy (SEM) in both Secondary and Back Scattered-Electron (SE and BSE) imaging modes plus microanalyses of inclusions were carried out by using a scanning electron microscope, model Hitachi S 4800 J (Hitachi Ltd., Chiyoda, Tokyo, Japan) with an Energy Dispersive X-ray Spectroscopy (EDS, Oxford INCA (Oxford Instruments plc., Abington, Oxfordshire, UK) capability. Similar to OM inspection, inclusion characterization by SEM was done on the polished samples.

Transmission Electron Microscopy (TEM) observations were carried out using a microscope model JEOL JEM 3000F (JEOL Ltd., Tokyo, Japan) equipped with an EDS unit (Oxford INCA) for elemental analyses. The samples were prepared from 3 mm diameter discs ground to ~80 μm thickness and then electropolished by Tenupol 5 (Struers Aps, Ballerup, Denmark) using 95/5: acetic/perchloric acid electrolyte at room temperature and the voltage of 40 V.
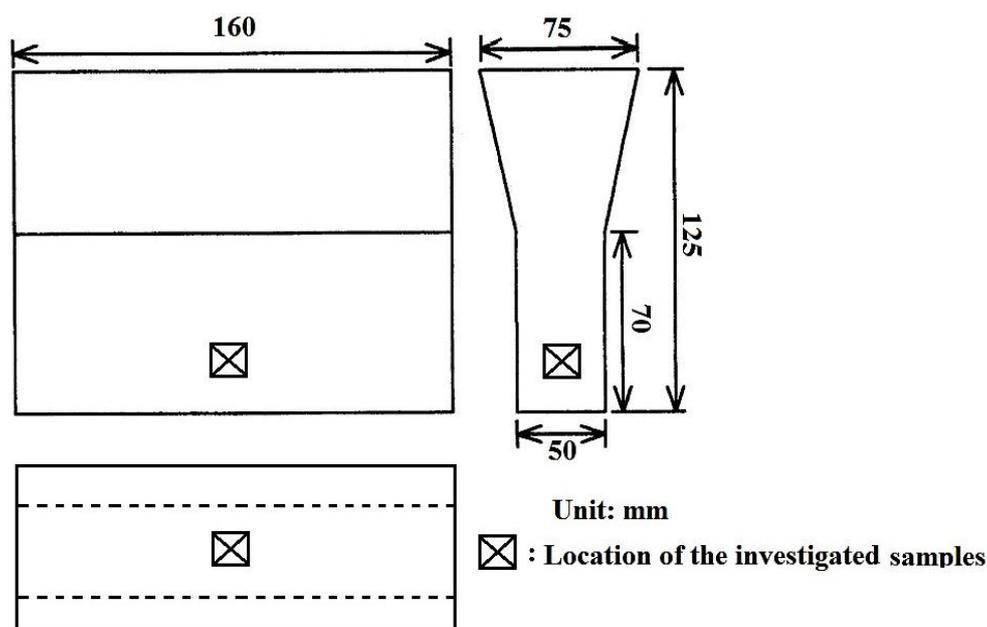
Figure 1. Scheme of the Y-block ingot and the location of investigated sample in it.

3. Results

3.1. OM Observations and Image Analyses of the Inclusions

Figure 2 shows characteristic optical images of distribution of the inclusions in different polished samples for steels R1, R2, R3 and R4, respectively. The average area fraction, average surface area and average roundness factor of the inclusions for the different steels are given in Table 5. These parameters were calculated from the images similar to those shown in Figure 3.

Considering the errors reported in Table 5, these values comprise of standard error (E) and also the errors imposed by the holes/gaps appeared on the polished surface. The value of E was calculated from the standard deviation (σ) and the number of measured inclusions (n) according to American Society for Testing and Materials (ASTM E2586): $E = \sigma/\sqrt{n}$. It should be noted that the average area of the inclusions have been estimated with respect to the total area covered by the inclusions and also the gaps appeared around some of the inclusions in the microstructure. It is very difficult to conclude whether the black particles, appeared in the OM images, are inclusions or pores. From the OM images, the gaps are not easily distinguishable as they appear with a similar color/contrast as the inclusions. However, they can be better differentiated in the SEM images, especially when using both SE and BSE imaging modes. The area covered by these gaps has been estimated and considered in calculation of the error of the reported results. The gaps themselves can be divided into two groups: (i) those caused during cooling by different thermal expansion coefficient between the inclusion and matrix; and (ii) those in which a broken part of an inclusion has been removed (a broken MnS particle as an example). This latter case has been avoided in this work by undertaking a careful metallographic preparation of the samples (which has been described in Section 2.2) and its contribution can be regarded as negligible. By considering the area covered by the gaps and by undertaking this correction, the intention of the authors has been to give the most accurate value for the area fraction of the inclusions. It should be noted that the gaps caused by thermal contraction have been more often observed in RE1 and RE2 rather than RE3 and RE4 steels. However, because of the reasons mentioned, there might be a minor error in the results of RE1 and RE2. The sum of the error given in Table 5 represents ≤5% of the average value measured for each sample.

It is known that area fraction/volume fraction (V) and mean diameter (dm) of the particles would affect the magnitude of mean free path (λ) between those particles according to Equations (1) and (2) [22–24], both of which result in a larger mean free path between the inclusions for the data obtained for steel RE3. According to Equation 1, this value was calculated to be around 12.4, 11.6, 14.1 and 11.4 μm for the data obtained for steels RE1, RE2, RE3 and RE4, respectively:

$$\lambda = \frac{4(1-V)}{3V}dm, \tag{1}$$

$$\lambda = \frac{(1-V)}{V}dm. \tag{2}$$

In addition, the results in this table also show that inclusions in samples RE3 and RE4 have an average roundness factor closer to 1 compared to the steels RE1 and RE2. This is clearly depicted in the images shown at higher magnification in Figure 3; these optical micrographs show that in RE1 (sample without RE) and RE2 (sample with 55 ppm RE), the roundness of inclusions is low (Figure 3a,b) while the roundness of the particles in RE3 and RE4 samples is closer to 1 (Figure 3c,d). It should be noted that, although the difference between average roundness factors is about 10–15 percent, the micrographs show a remarkable difference in roundness factor for the coarser inclusions. This is due to the fact that small inclusions in all samples look spherical (with roundness close to 1), which would affect the magnitude of the average roundness factor of inclusions for the different samples. Furthermore, in the micrographs shown in Figure 3, dark areas surrounded by gray envelope can be distinguished almost in all cases.
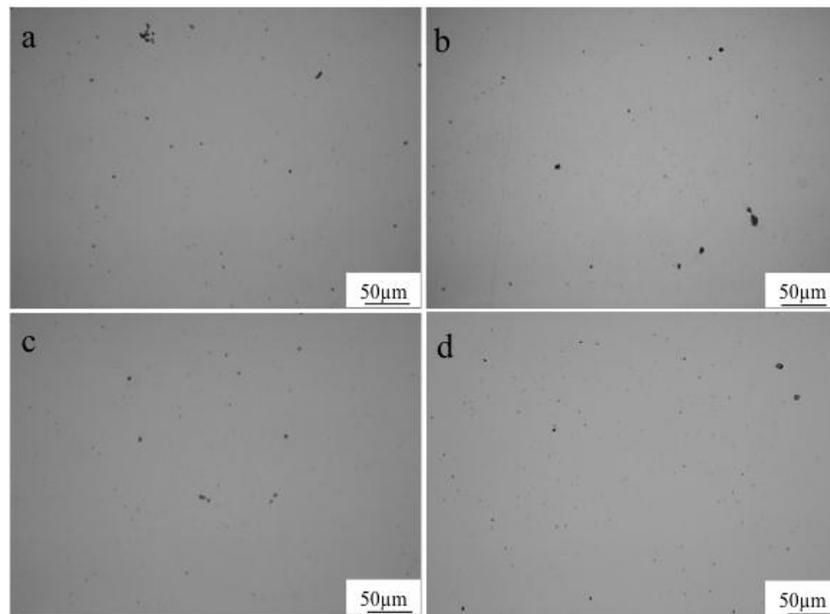
Figure 2. Optical micrographs showing the characteristic distribution of inclusions in steels: (**a**) RE1, (**b**) RE2, (**c**) RE3 and (**d**) RE4.

Table 5. Inclusion characteristics in different samples.

Steels	Area Fraction, %	Average Area, (μm^2)	Average Size, (μm)	Average Roundness Factor
RE1	0.123 ± 0.004	1.35 ± 0.06	1.31	0.71 ± 0.02
RE2	0.138 ± 0.005	1.54 ± 0.07	1.40	0.74 ± 0.03
RE3	0.105 ± 0.004	1.21 ± 0.04	1.24	0.83 ± 0.02
RE4	0.134 ± 0.005	1.38 ± 0.05	1.32	0.82 ± 0.03
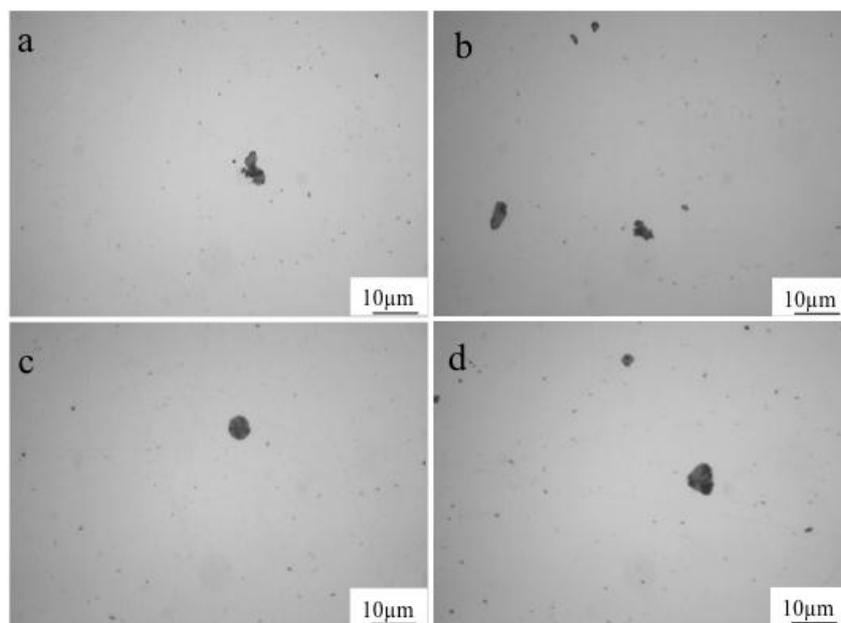
Figure 3. Morphologies and distribution of inclusions in steels: (**a**) RE1, (**b**) RE2, (**c**) RE3 and (**d**) RE4 at higher magnification.

3.2. Inclusion Characterization by SEM

3.2.1. Sample RE1

Figure 4 shows SEM images of characteristic inclusions observed in sample RE1 along with their microanalyses. It can be seen in Figure 4a that the roundness of the inclusion particles is low. In addition, in this figure, black areas could be considered as a gap/hole between the inclusion and the matrix. These gaps have been reported as one of the reasons for steels susceptibility to brittleness [25]. Figure 4b (spectrum No. 4) shows a considerable accumulation of Nb in the vicinity of these inclusions. A detailed evaluation of the larger inclusions in this sample using SE and BSE imaging modes (Figure 5a,b) revealed that there are white areas around the MnS particles. Microanalyses of these areas illustrate that there exist aggregations of Nb-rich phases (likely NbC) on the surface of MnS particle (Figure 5c). It is important to be mentioned that the use of Wavelength Dispersive Spectroscopy (WDS) should be considered if better limits of detection or accurate and precision performance is searched for light elements (C, O, N); thus, the results obtained for the light elements should be taken with caution.

The elemental distribution map of an inclusion in RE1 (Figure 6) confirms the accumulation of considerable amounts of Nb around the MnS. In addition, the micrographs show an Al_2O_3 inclusion surrounded by a MnS particle, which suggests the possibility of MnS nucleation on these oxides. This type of synergy between Al_2O_3 and MnS particles has been often observed in the microstructures. It is noteworthy that, for the steels deoxidized with aluminum, Al_2O_3 particles exist as non-metallic inclusions having unique faceted shapes, clusters of which tend to remain in solidified steels [26]. Apart from the Al_2O_3, another dark area can be seen in the bottom left part of this inclusion, which, according to the microanalyses, is suggested to be an Si-oxide particle probably originated from casting in the sand mold. As it can be seen, some parts around this particle have been probably removed during the preparation process.

b)

Spectrum	Chemical composition, Wt. %						
	O	Al	Si	Mn	Fe	Nb	C
1	36.72	36.91	-	-	26.38	-	-
2	41.55	20.66	0.55	13.39	18.42	-	-
3	-	-	0.48	1.25	94.08	-	4.18
4	14.99	5.20	0.67	-	74.33	1.20	2.79
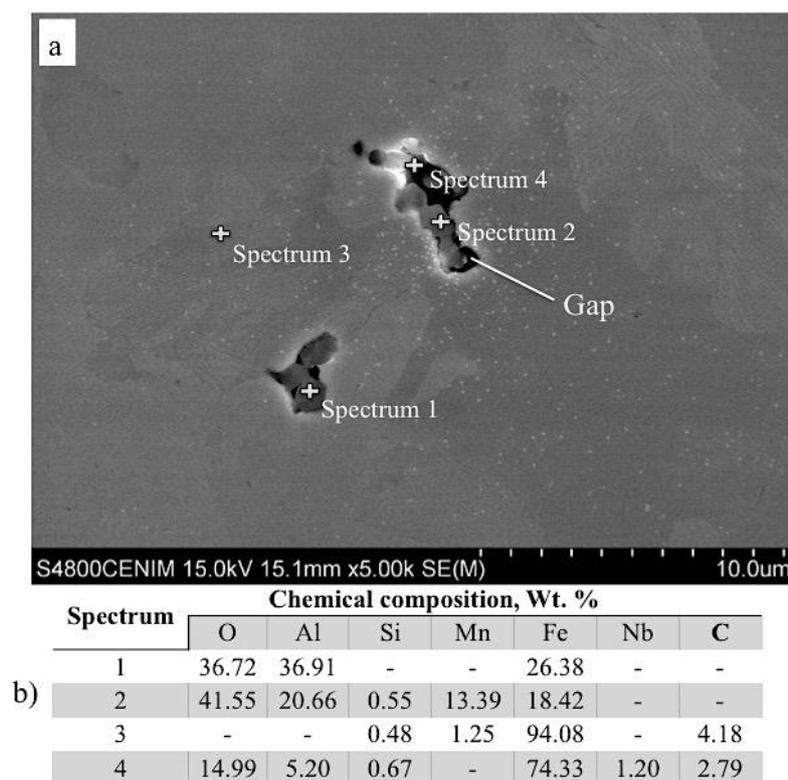
Figure 4. (**a**) SEM (Scanning Electron Microscopy) micrograph and (**b**) EDS (Energy Dispersive X-ray Spectroscopy) results of the inclusions in steel RE1.

	Spectrum	Chemical composition, Wt. %							
		O	Al	V	Mn	S	Fe	Nb	C
c)	1	-	-	1.21	1.03	-	19.50	65.52	12.73
	2	-	-	-	57.59	33.41	2.72	-	5.66
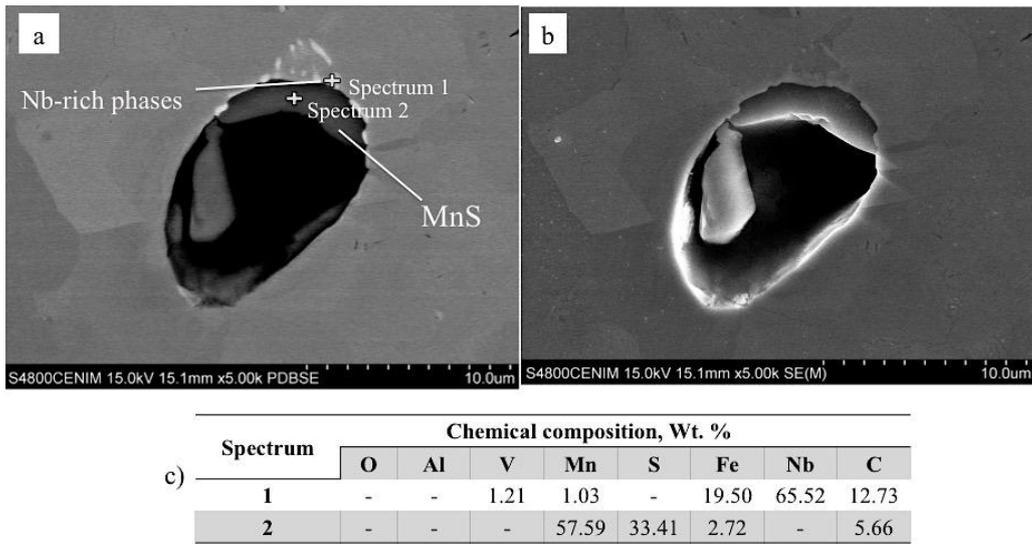
Figure 5. SEM micrographs in (**a**) BSE (Back Scattered Electron) and (**b**) SE (Secondary Electron) modes and (**c**) the results of EDS analysis of the inclusion observed in steel RE1.
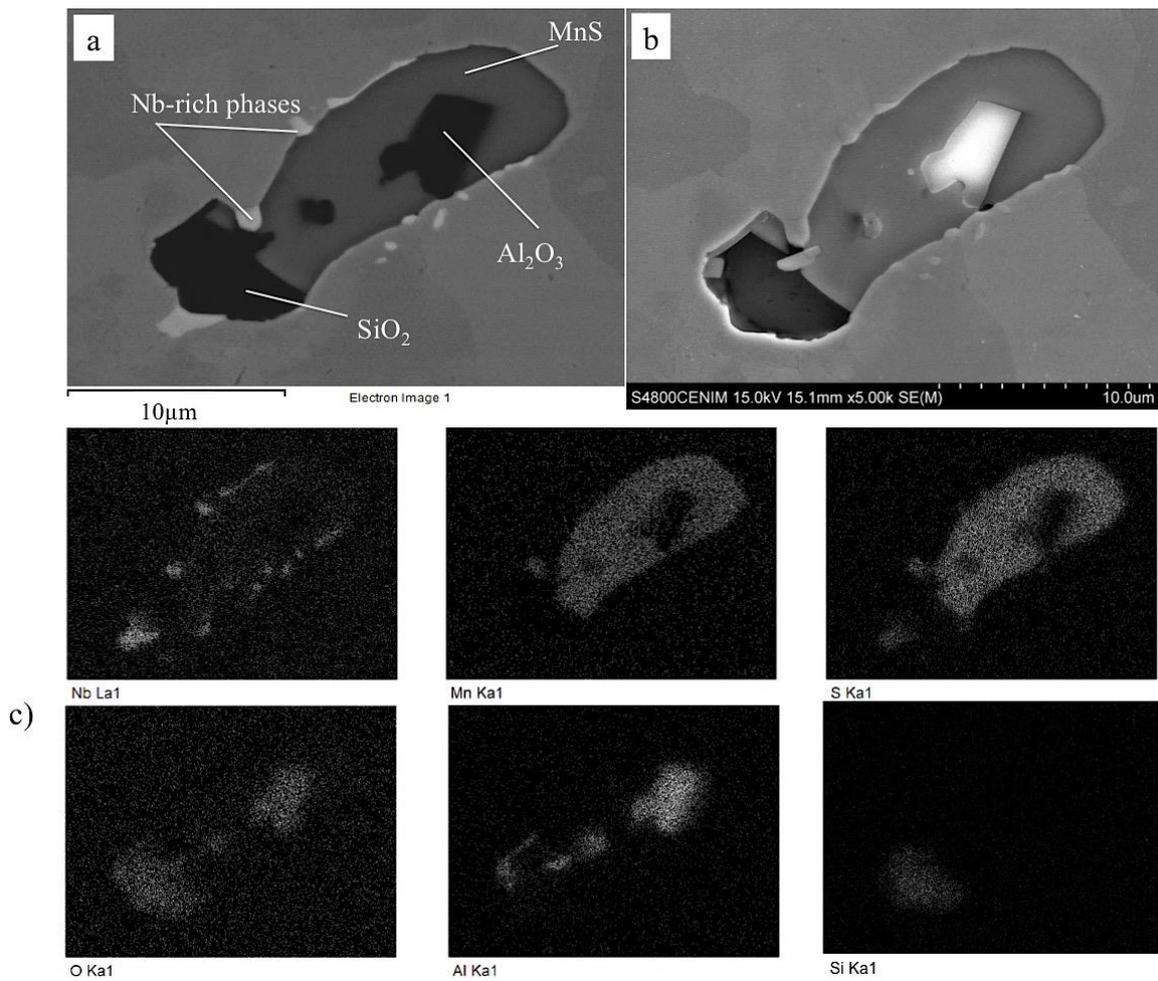
Figure 6. (**a**) BSE and (**b**) SE images of inclusion appeared in steel RE1 and (**c**) its elemental mapping.

3.2.2. Sample RE2

Figure 7 shows the SEM images and elemental map of an inclusion in sample RE2. Despite the addition of RE to this sample, there is not a significant change in the nature of inclusions; MnS could be considered as a dominant inclusion surrounding Al_2O_3. According to the elemental mappings, the existence of (La,Ce)-rich phases in the vicinity of Al-oxide would unveil the possibility of formation of these components on the preexisted Al_2O_3. Similar to steel RE1, precipitation of considerable amount of Nb-rich phases (white area) can be clearly seen around MnS in this steel (Figure 7a). Finding these NbC precipitates at the surface of MnS inclusions was not surprising, as the elements like Al, Mn, La or Ce form inclusions (oxy-sulphides) in the melt or in the pasty region first, while NbC particles would nucleate and grow/coarsen after the formation of these inclusions has taken place.
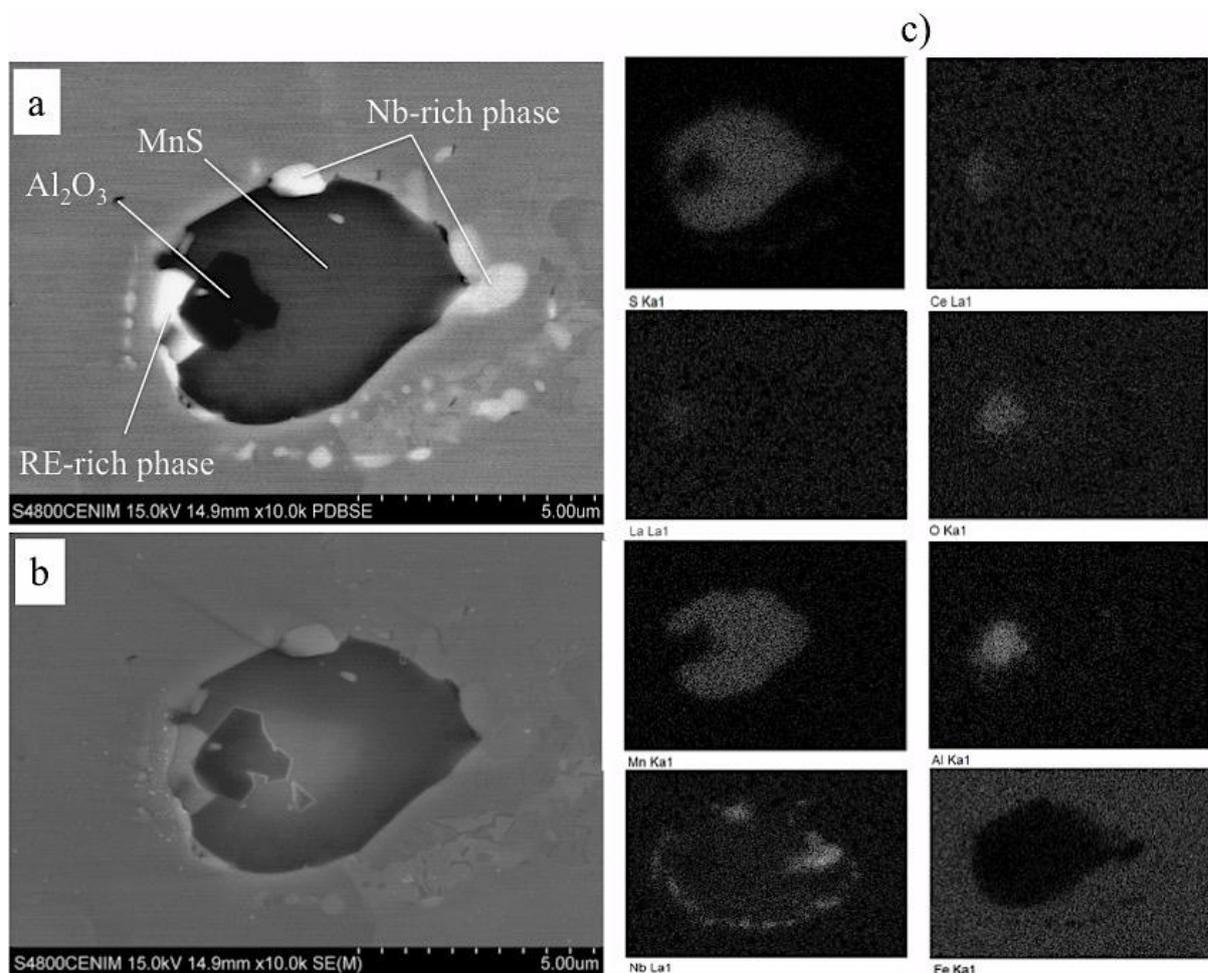
Figure 7. SEM micrographs in (**a**) BSE and (**b**) SE imaging modes of an inclusion appeared in steel RE2 and (**c**) its elemental mappings.

3.2.3. Samples RE3 and RE4

Figure 8 illustrates a complex inclusion observed in the microstructure of sample RE3. According to the microanalyses (elemental map), this complex inclusion is mainly composed of a cluster of cubic light particles all over this inclusion. Due to the high content in La, Ce, Al and O of these cubic particles, they seem to be (RE,Al)-based oxides (likely $(RE,Al)_2O_3$). The results of the EDS microanalysis performed on one of these cubic (Figure 8d) approve that due to the high oxygen content, the cubic light particles are oxides as labeled in Figure 8a. Previous reports indicated and discussed the agglomeration tendency of these cubic inclusions to lower the contact area with molten

steel [26]. In addition, some small gray particles can be seen in SEM images, which are based on the microanalyses, are believed to be (RE,Mn)S. In addition to these particles, a darker phase similar to those observed in Figures 6 and 7 can be distinguished in this complex inclusion, which, according to the elemental mappings, is proposed to be Al_2O_3 type. These particles are distributed in the matrix of this inclusion, which seems to consist of RE-sulfides. Despite the addition of RE to sample RE2, such a complex inclusion has not been observed in that sample. Regarding the complex inclusion illustrated in Figure 8, there is no sign of Nb-rich areas in the outer surface of the inclusions, which have been noticed in RE1 and RE2 (Figures 5–7). It is worth mentioning that, although the Mn-containing particles co-exist with Al_2O_3 in RE1, RE2 and RE3, in the latter steel, the presence of Mn is much scarcer.

A characteristic inclusion in sample RE4 and its microanalyses are illustrated in Figure 9. As observed in steel RE3, the EDS analysis shows the co-existence of Al_2O_3 particles with RE inclusions in sample RE4. It should be also mentioned that in this sample the presence of Mn could not be detected as part of the inclusion composition, suggesting that MnS has not been formed (Figure 9c) in this sample. This is possibly due to the fact that sulfur has been linked to La/Ce and there is little sulfur available for the formation of MnS. In fact, when RE consumes S to form RE(S,O)/RES, the content of S in solid solution as well as its activity will be decreased, lowering the possibility of MnS formation in the presence of RE. Thus, it can be proposed that the rest of the sulfur exists in the form of solid solution in the matrix. In addition, in a similar way as for RE3, inclusions in sample RE4 do not show the accumulation of Nb on the inclusion–matrix interfaces.

Spectrum	Chemical composition, Wt. %								
	O	Al	S	Mn	Fe	V	La	Ce	C
1	22.93	9.98	0.05	-	1.95	0.21	14.49	46.44	4.04
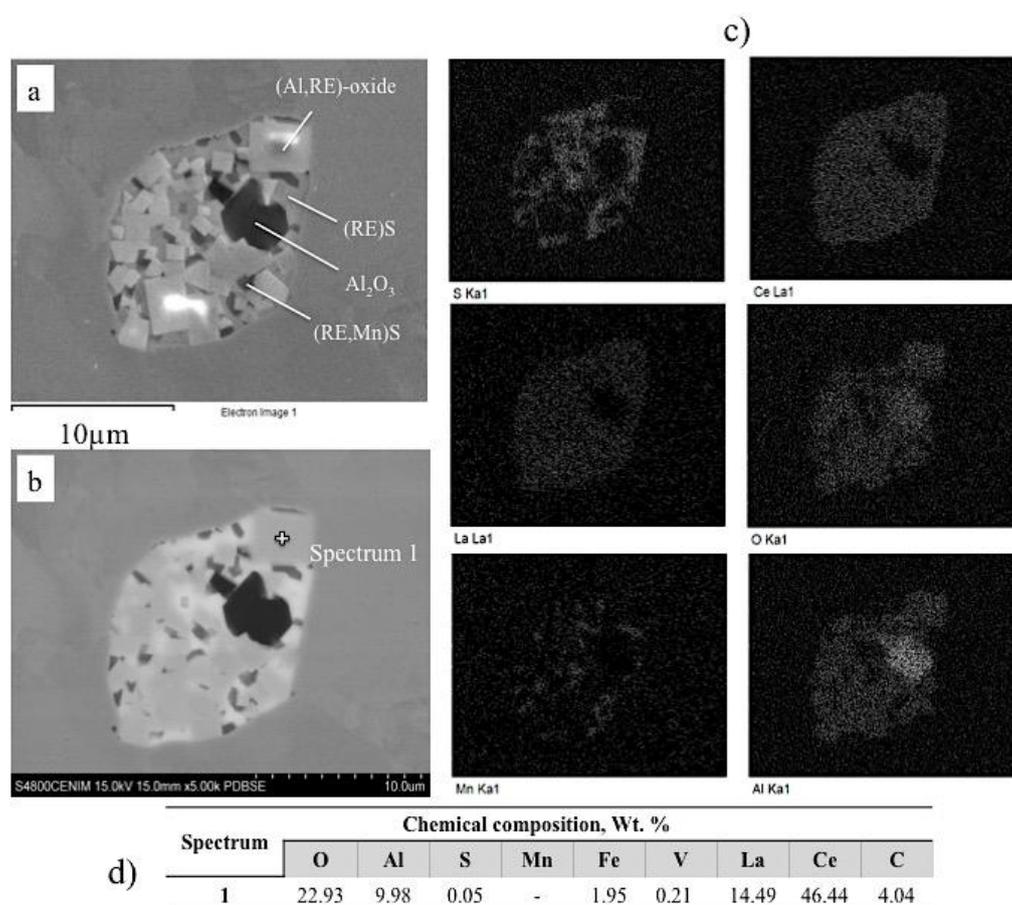
Figure 8. SEM micrographs in (**a**) SE and (**b**) BSE modes of a complex inclusion modified by 199.5 ppm RE, (**c**) elemental map of the corresponding inclusion in RE3 steel, and (**d**) the EDS results of spectrum 1.

Spectrum	Chemical composition, Wt. %						
	O	Al	S	Fe	Ce	La	C
1	39.56	28.77	1.30	1.39	11.52	8.16	7.16
2	1.83	0.97	19.17	2.65	41.40	21.89	12.07
3	12.07	5.04	7.65	5.32	38.73	20.23	11.28
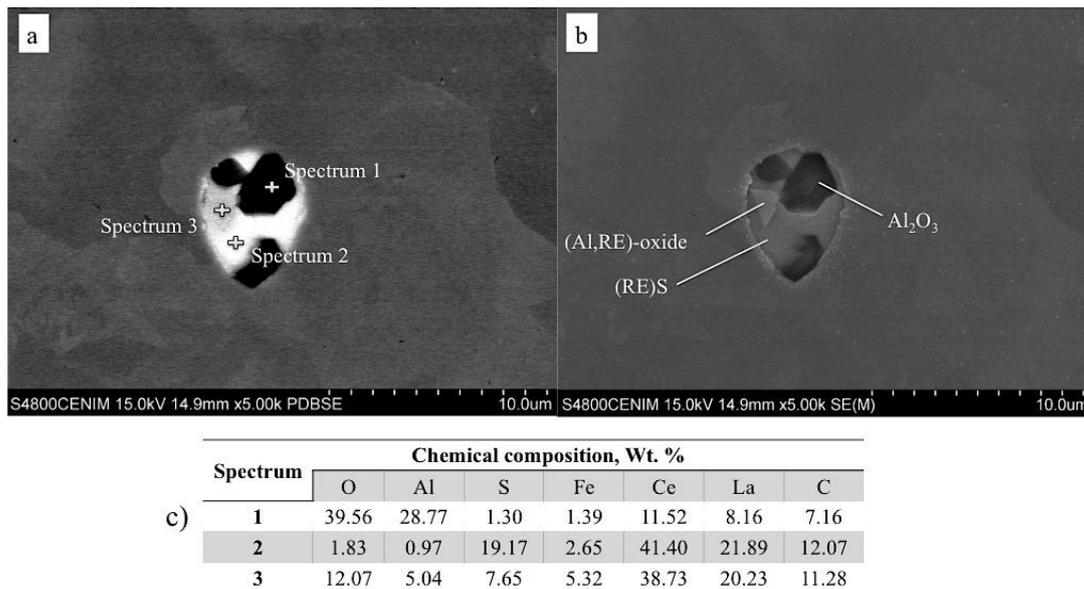
Figure 9. SEM micrograph in (**a**) BSE and (**b**) SE modes, (**c**) EDS analysis of a complex inclusion observed in steel RE4.

4. Discussion

4.1. Nature of Inclusions: Volume Fraction, Size and Roundness

In order to complement and discuss the results obtained in this investigation, equilibrium phases and their transformation temperature ranges were calculated by means of Thermo-Calc® (Solna, Sweden), which is a thermodynamic software based on the CALPHAD (Computer Coupling of Phase Diagrams and Thermo-chemistry), using TCFE8 database and using the chemical composition of the base steel (Table 3). It should be mentioned that the database does not contain information regarding the influence of RE elements on equilibrium phase formation. Although these simulations do not take into account the influence of RE-alloying elements, they still give very useful information to understand some of the experimental observations presented in this investigation.

Figure 10 reveals that Al_2O_3 exists in the molten steel at temperatures even above 1500 °C, but MnS is present at the lower temperature range of the pasty region (<1464 °C). These data predict that, during solidification, alumina (Al_2O_3) would be formed first, followed by MnS. This sequence of formation would explain observations like that provided in Figure 6; alumina inclusions already present in the molten steel at high temperatures would be used as nucleation sites by MnS particles, which do form at lower temperatures. As a result, complex inclusions with an inner alumina core and MnS crust would be formed.

As it has been mentioned above, the Gibbs free energy of the formation of RE sulfides is so negative (Table 1); thus, these components form right after the RE addition into the molten steel. It seems that 55 ppm addition of RE into the steel (RE2) was not sufficient to consume a considerable amount of the sulfur in molten steel and, thus, some free sulfur also combined with Mn to promote the formation of MnS in RE2 (same as in RE1). Higher level of RE additions (RE3 and RE4) would lead to almost the complete consumption of the sulfur to form sulfides or oxysulphides, reducing the concentration of free sulfur in the molten steel considerably. In this case, the amount of sulfur available to form MnS, would be negligible, which could explain why this inclusion can hardly be found in steel RE3 (Figure 8) or has not been observed in the analysis presented in Figure 9. In other words, when the amount of RE addition is high enough to consume the entire or considerable amount of sulfur, the formation of MnS would be avoided and all the Mn would remain in solid solution.
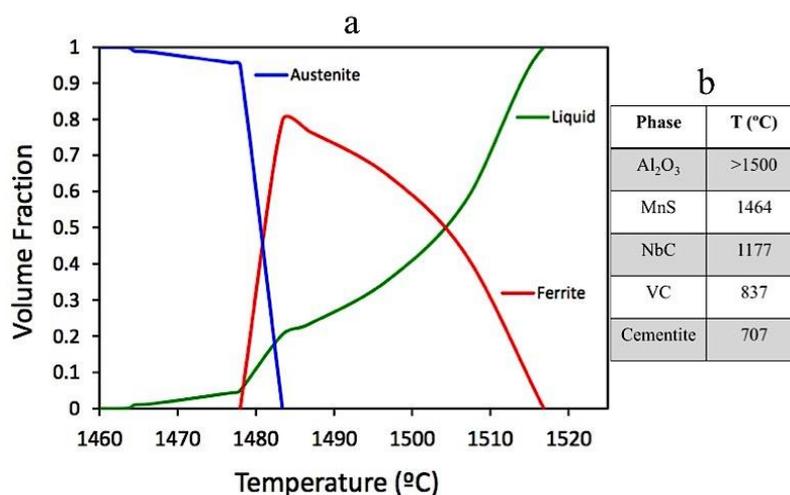
Figure 10. (**a**) equilibrium phases and solidification temperature range and (**b**) maximum temperature at which different equilibrium phases are present in the base steel according to Thermo-Calc predictions.

It was shown in Table 5 that, in comparison with the base steel, a low level of RE addition (55 ppm, RE2) results in having a higher area fraction of inclusions with a larger size while a higher level of rare earth addition (199.5 ppm, RE3) could decrease both their area fraction and average size. The same results (higher fraction of inclusions with low level of RE addition) has been reported earlier [10], where the authors claimed that this outcome would be contributed to the floatability of the inclusions (oxides, sulfides and oxy-sulphides) in the presence of RE and also to the location in the ingot from which the studied samples have been taken. In fact, the modification of the oxide inclusions to oxysulphides improves their floatability because of the lower density of oxysulphides/sulfides compared to oxides. Hence, with the formation of RE sulfides/oxysulphides, especially regarding the modification of Al_2O_3 clusters, RE3 steel achieved the lowest area fraction of inclusions by promoting the floatability of inclusions towards upper part of the ingot (this kind of complex inclusion that has been trapped during solidification is shown in Figure 8). In steel RE4, it seems that an excessive amount of RE has promoted a higher area fraction of inclusions with a larger average size, which could be caused by the higher activity of RE elements. Considering the cleanliness and associated mechanical properties of steels, it has been pointed out that the excessive amount of RE in steel should be avoided [5,25].

In this case, for the investigated type of microalloyed steel, it seems that 200 ppm of RE would be enough in order to avoid the formation of MnS as preferential sites for Nb accumulation and reach a high roundness factor. A higher level of RE addition beyond this amount would result, as discussed before, in having a greater volume fraction of inclusions with larger size, which is detrimental for steel properties [3].

In addition, it was found that, in comparison with the inclusions observed in samples RE1 and RE2, the roundness factor of inclusions in RE3 and RE4 is closer to 1, which could be attributed to the formation of RE(S,O)-Al_2O_3 inclusions in the molten steel and reaching the minimum surface energy with the melt [23].

4.2. Influence of RE Addition on the Accumulation of Nb-Rich Phases Around MnS and Nanoprecipitation

It is well documented that, among the microalloying elements, Nb plays the most important role as a solid solution strengthener and it also forms very fine precipitates in the matrix that can contribute to grain refinement and precipitation hardening in the microalloyed steels [27–35]. Therefore, the formation of coarse Nb(C,N) precipitates would reduce the amount of Nb available in solid solution to strengthen through nanoprecipitation. As it has been shown previously, it is evident that Nb accumulates around MnS in RE1 and RE2 samples (Figures 5–7), likely forming large NbC and/or

Nb(C,N) precipitates. According to the thermodynamic calculations, NbC precipitates form in the solid state (austenite) below ~1177 °C (Figure 10).

In addition, it is known that the presence of heterogeneous nucleation sites in the matrix, like MnS inclusions for Nb-rich phases, can even alter the formation range of Nb(C,N) precipitates, shifting it to higher temperatures [23]. To dissolve these primary large Nb-rich carbonitrides, the steel would have to be heated to very high temperatures [36], which is not always easy to reach. In contrast to MnS particles observed in steels RE1 and RE2, (La,Ce)(S,O)-Al$_2$O$_3$ inclusions do not seem to be preferential sites for Nb(C,N) nucleation in steels RE3 and RE4 (Figures 8 and 9).

The presence of the nanoprecipitates in the matrix has been characterized by TEM in steels RE2 and RE3. Figure 11 reveals the presence of few V-rich precipitates in the microstructure of sample RE2; these precipitates are also rich in Nb, which suggests that complex (Nb,V)(C,N) precipitates have been formed. According to the thermodynamic calculations, V-rich precipitates would only form at temperatures much lower than that of Nb(C,N) (<837 °C). As it has been shown in Figure 7, large Nb(C,N) particles have precipitated at the surface of MnS inclusions in steel RE2, reducing the amount of Nb in solid solution available to promote nanoprecipitates in the steel matrix, which is the reason why they have not been detected so easily in this steel. In contrast to RE2, large Nb(C,N) precipitates have not been observed at inclusion surfaces and the microstructure of RE3 sample shows the presence of several Nb-rich precipitates (Figure 12). These precipitates are also rich in V, although its presence is much lower than Nb. As mentioned above, previous studies [20,21] have suggested that RE addition increases the amount of Nb dissolved in solid solution in the austenite, which would allow forming Nb(C,N) nanoprecipitates during cooling in the matrix.

There is limited information in the literature concerned with the mechanism by which RE addition could affect the formation of NbC precipitates in steels. However, the present results suggest that its formation is associated with the presence of MnS inclusions in the microstructure. The addition of significant concentrations of RE elements in RE3 and RE4 samples would promote the formation of (La,Ce)(O,S) inclusions in the melt and the removal of the sulfur from solid solution. As a consequence, the formation of MnS is inhibited (no sulfur available in solution) and the formation of coarse Nb-rich phases is avoided, as these do not seem to form at the surface of (La,Ce)(O,S) and only at MnS inclusions.

Element	Atomic %
Fe	74.73
Nb	6.57
V	17.54
Mn	1.12
Ti	0.04
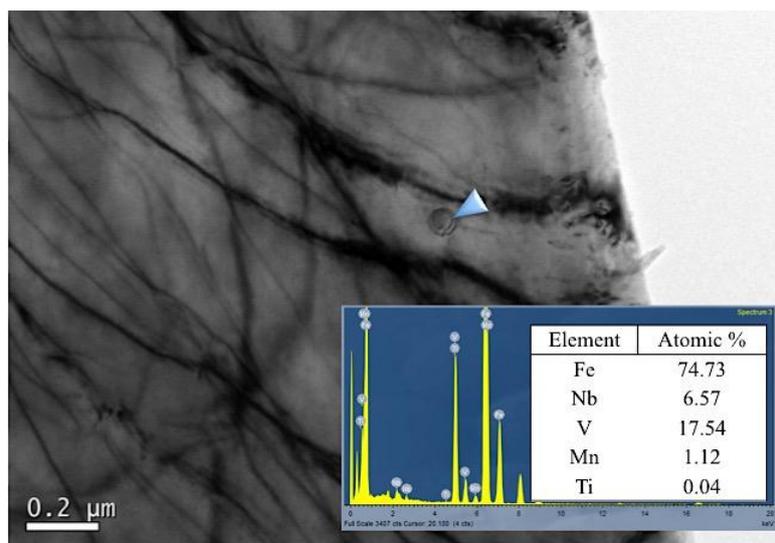
Figure 11. TEM (Transmission Electron Microscopy) micrograph of steel RE2 presenting V-rich precipitate along with its EDS microanalysis.
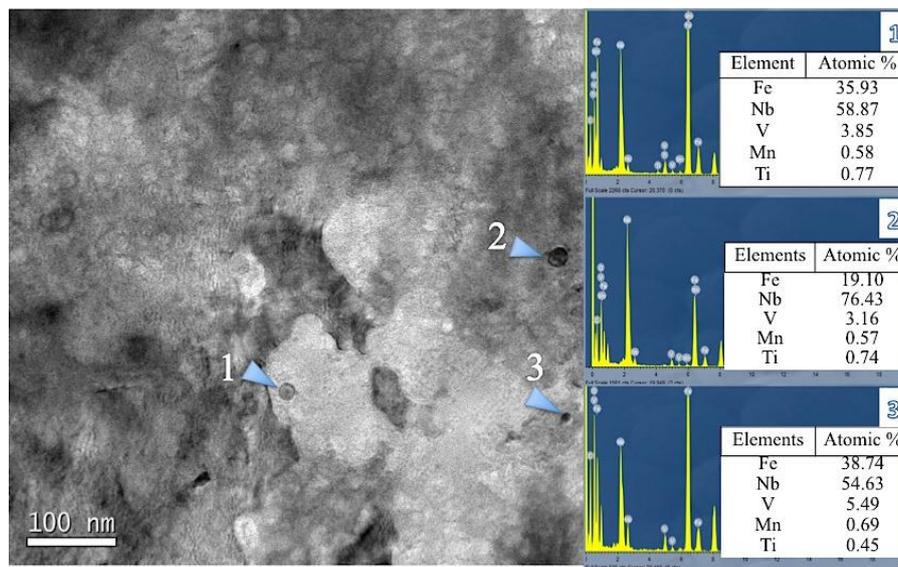
Figure 12. TEM micrograph of steel RE3 presenting Nb-rich precipitates along with their EDS microanalysis.

It is known that the difference between the thermal contraction of inclusions and the matrix during cooling can create stress fields around the inclusions leading to the adjacent matrix deformation or discontinuity between the matrix and inclusion [37–39]. Figure 13 illustrates the thermal expansion coefficients of conventional inclusions and includes data from different references [40–42]. This figure has been copied, with permission, from Figure 10 in reference [43]. If the thermal expansion coefficient of an inclusion is lower than that of the matrix (ferrite), like that of Al_2O_3, stress fields appear around the inclusions; however, in the case of higher contraction coefficient than ferrite e.g. MnS, vacancies and subsequently gaps could appear [37]. It can be seen that MnS has one of the highest values among the typical inclusions while Al_2O_3 and other oxides have lower values. It is worth mentioning that the thermal expansion coefficient of ferrite lies between the values for MnS and Al_2O_3, which is reported to be around 11×10^{-6} (1/°C) [44]. In addition, based on the ThermoCalc predictions (Figure 10), the investigated steels are hyper-peritectic type; i.e., delta ferrite is the first phase that solidifies from molten steel during cooling. In addition, MnS has been found to form in the lower range of the pasty region. It is known that the solubility of sulfur in molten steel is higher than the solid state, so, as solidification proceeds, the sulfur concentration would build up in the remained molten steel, resulting in higher sulfide formation [26]. In addition, non-equilibrium condition/heterogeneous nucleation can alter the formation temperature of MnS to higher temperature. Both phenomena would lead to the formation of MnS in the temperature range where delta ferrite coexists with the molten steel. In other words, the proposed mechanism considers the difference between the thermal expansion coefficient of MnS and the delta ferrite, while when it is compared with that of austenite, such a difference does not exist. For RE-based inclusions, this factor has been reported to be similar to that of ferrite [38,45]. Eventually, due to the considerable difference between the thermal contraction of MnS and delta ferrite, MnS creates stress fields at its interface with matrix as well as losing its solid continuity, which is likely to remain even after transformation of delta ferrite to austenite. Thus, these areas could provide preferential sites for Nb accumulation/precipitation at high temperature, as it has been experimentally observed in this investigation.
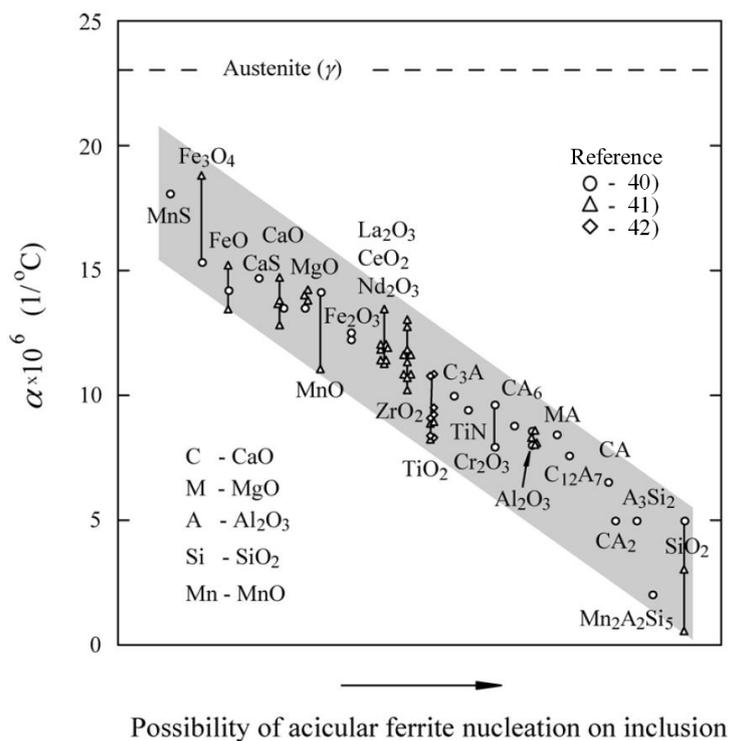
Figure 13. Thermal expansion coefficient of conventional inclusions found in steels; this Figure has been copied from Figure 10 in reference [43].

5. Conclusions

The major findings of the present investigation have been highlighted as follows: according to SEM results, RE addition can change the nature of inclusions formed during casting. In the base and low RE-added steels, Al_2O_3 exists in the molten steel and MnS inclusions form in the pasty region at lower temperatures, sometimes nucleating at these alumina particles and forming complex inclusions. Higher level of RE additions to the base steel (RE3 and RE4) promotes the formation of inclusions with an RE-based matrix instead of Al_2O_3-MnS inclusions that can modify the Al_2O_3 cluster as well.

The results of image analyses showed that the inclusions observed in RE3 and RE4 are rounder than those Al_2O_3-MnS found in RE1 and RE2. The rest of parameters e.g., area fraction and size of the inclusions did not follow a clear trend; compared to RE3, inclusions in steel RE4 were larger with higher area fraction that can lead to poor mechanical properties.

Formation of MnS was suppressed in steels RE3 and RE4, which has been found to serve as preferential sites for the precipitation of Nb-rich phases. As a consequence, alloying the steel with more than 200 ppm of RE inhibited the formation of coarse Nb-based precipitates. Thus, Nb remains in solid solution and available for nanoprecipitation as NbCN.

The precipitation of Nb-rich phases on MnS inclusions would be due to the difference in the thermal expansion coefficient between the matrix and the MnS particles. This difference could cause stress fields as well as solid discontinuity at the interface of MnS with matrix during cooling providing nucleation sites for Nb-rich phases.

References

1. Thornton, P.A. The influence of nonmetallic inclusions on the mechanical properties of steel: A review. *J. Mater. Sci.* **1971**, *6*, 347–356. [CrossRef]

2. Bytyqi, A.; Puksic, N.; Jenko, M.; Godec, M. Characterization of the inclusions in spring steel using light microscopy and scanning electron microscopy. *Mater. Tehnol.* **2011**, *45*, 55–59.

3. Zhang, L.; Thomas, B.G. State of the art in the control of inclusions during steel ingot casting. *Metall. Mater. Trans. B* **2006**, *37*, 733–761. [CrossRef]

4. Shi, G.; Zhou, S.; Ding, P. Investigation of nonmetallic inclusions in high-speed steels. *Mater. Charact.* **1997**, *38*, 19–23. [CrossRef]

5. Gao, J.; Fu, P.; Liu, H.; Li, D. Effects of rare earth on the microstructure and impact toughness of H13 steel. *Metals* **2015**, *5*, 383–394. [CrossRef]

6. Senberger, J.; Cech, J.; Zadera, A. Influence of compound deoxidation of steel with Al, Zr, rare earth metals, and Ti on properties of heavy castings. *Arch. Foundry Eng.* **2012**, *12*, 99–104. [CrossRef]

7. Opiela, M.; Kamińska, M. Influence of the rare-earth elements on the morphology of non-metallic inclusions in microalloyed steels. *JAMME* **2011**, *47*, 149–156.

8. Wang, L.M.; Lin, Q.; Yue, L.J.; Liu, L.; Guo, F.; Wang, F.M. Study of application of rare earth elements in advanced low alloy steels. *J. Alloy. Compd.* **2008**, *451*, 534–537. [CrossRef]

9. Grajcar, A.; Kaminska, M.; Galisz, U.; Bulkowski, L.; Opiela, M.; Skrzypczyk, P. Modification of non-metallic inclusions in high-strength steels containing increased Mn and Al contents. *JAMME* **2012**, *55*, 245–255.

10. Paul, S.K.; Chakrabarty, A.K.; Basu, S. Effect of rare earth additions on the inclusions and properties of a Ca-Al deoxidized steel. *Metall. Trans. B* **1982**, *13*, 185–192. [CrossRef]

11. Opiela, M.; Grajcar, A. Modification of non-metallic inclusions by rare-earth elements in microalloyed steels. *Arch. Foundry Eng.* **2012**, *12*, 129–134. [CrossRef]

12. Kimanov, B.M. Removing oxide and sulfide inclusions from molten steel by filtration. *Steel Transl.* **2008**, *38*, 641–646. [CrossRef]

13. Vahed, A.; Kay, D.A.R. Thermodynamics of rare earths in steelmaking. *Metall. Trans. B* **1976**, *7*, 375–383. [CrossRef]

14. Wu, Y.; Wang, L.; Du, T. Thermodynamics of rare earth elements in liquid iron. *J. Less Common Met.* **1985**, *110*, 187–193. [CrossRef]

15. Garrison, M.W., Jr.; Maloney, L.J. Lanthanum additions and the toughness of ultra-high strength steels and the determination of appropriate lanthanum additions. *Mater. Sci. Eng. A* **2005**, *403*, 299–310.

16. Akila, R.; Jacob, K.T.; Shukla, A.K. Gibbs energies of formation of rare earth oxysulfides. *Metall. Trans. B* **1987**, *18*, 163–168. [CrossRef]

17. Ma, Q.; Wu, C.; Cheng, G.; Li, F. Characteristic and formation mechanism of inclusions in 2205 duplex stainless steel containing rare earth elements. *Mater. Today Proc.* **2015**, *2*, 300–305. [CrossRef]

18. Handerhan, K.J.; Garrison, W.M. Effects of rare earth additions on the mechanical properties of the secondary hardening steel AF1410. *Scr. Metall.* **1988**, *22*, 409–412. [CrossRef]

19. Belyakova, A.F.; Kryankovskii, Y.V.; Paisov, I.V. Effect of rare earth metals on the structure and properties of structural steel. *Met. Sci. Heat Treat.* **1965**, *7*, 588–593. [CrossRef]

20. Liu, H.-L.; Liu, C.-J.; Jiang, M.-F. Effect of rare earths on impact toughness of a low-carbon steel. *Mater. Des.* **2012**, *33*, 306–312. [CrossRef]

21. Liu, H.L.; Liu, C.J.; Jiang, M.F. Effects of rare earths on the austenite recrystallization behavior in X80 pipeline steel. *Adv. Mater. Res.* **2010**, *129–131*, 542–546. [CrossRef]

22. Muro, P.; Gimenez, S.; Iturriza, I. Sintering behaviour and fracture toughness characterization of D2 matrix tool steel, comparison with wrought and PM D2. *Scr. Mater.* **2002**, *46*, 369–373. [CrossRef]

23. Porter, D.A.; Easterling, K.E.; Sherif, M. *Phase Transformations in Metals and Alloys*, 3rd ed.; Revised Reprint; CRC Press: London, UK, 2009.

24. Torkamani, H.; Raygan, S.; Rassizadehghani, J. Comparing microstructure and mechanical properties of AISI D2 steel after bright hardening and oil quenching. *Mater. Des.* **2014**, *54*, 1049–1055. [CrossRef]

25. Kasińska, J. Influence of rare earth metals on microstructure and inclusions morphology G17CrMo5–5 cast steel. *Arch. Metall. Mater.* **2014**, *59*, 993–996. [CrossRef]

26. Muan, A.; Osborn, E.F. *Phase Equilibria Among Oxides in Steelmaking*; Addison-Wesley: Boston, MA, USA, 1965.

27. Davis, J.R. *Alloying: Understanding the Basics*; ASM International: Novelty, OH, USA, 2001; p. 647.

28. Najafi, H.; Rassizadehghani, J.; Asgari, S. As-cast mechanical properties of vanadium/niobium microalloyed steels. *Mater. Sci. Eng. A* **2008**, *486*, 1–7. [CrossRef]

29. Najafi, H.; Rassizadehghani, J.; Norouzi, S. Mechanical properties of as-cast microalloyed steels produced via investment casting. *Mater. Des.* **2011**, *32*, 656–663. [CrossRef]

30. Rassizadehghani, J.; Najafi, H.; Emamy, M.; Eslami-Saeen, G. Mechanical properties of V-, Nb-, and Ti-bearing as-cast microalloyed steels. *J. Mater. Sci. Technol.* **2007**, *23*, 779–784.

31. Sosnin, V.V.; Longinov, A.M.; Barantseva, I.V.; Povkova, N.A.; Lyasotskii, I.V. Distribution of niobium and titanium carbonitrides in continuous-cast microalloy steels. *Steel Transl.* **2010**, *40*, 590–594. [CrossRef]

32. Chen, C.Y.; Yen, H.W.; Kao, F.H.; Li, W.C.; Huang, C.Y.; Yang, J.R.; Wang, S.H. Precipitation hardening of high-strength low-alloy steels by nanometer-sized carbides. *Mater. Sci. Eng. A* **2009**, *499*, 162–166. [CrossRef]

33. San Martin, D.; Caballero, F.G.; Capdevila, C.; Garcia de Andres, C. Austenite grain coarsening under the influence of niobium carbonitrides. *Mater. Trans.* **2004**, *45*, 2797–2804.

34. Vivas, J.; Celada-Casero, C.; San Martín, D.; Serrano, M.; Urones-Garrote, E.; Adeva, P.; Aranda, M.M.; Capdevila, C. Nano-precipitation strengthened G91 by thermo-mechanical treatment optimization. *Metall. Mater. Trans. A* **2016**, *47*, 5344–5351. [CrossRef]

35. Mousavi Anijdan, S.H.; Rezaeian, A.; Yue, S. The effect of chemical composition and austenite conditioning on the transformation behavior of microalloyed steels. *Mater. Charact.* **2012**, *63*, 27–38. [CrossRef]

36. Vivas, J.; Capdevila, C.; Jimenez, J.; Benito-Alfonso, M.; San-Martin, D. Effect of ausforming temperature on the microstructure of G91 steel. *Metals* **2017**, *7*, 236. [CrossRef]

37. Sohaciu, M.; Predescu, C.; Vasile, E.; Matei, E.; Savastru, D.; Berbecaru, A. Influence of MnS inclusions in steel parts on fatigue resistence. *Dig. J. Nanomater. Biostruct.* **2013**, *8*, 367–376.

38. Drar, H. Metallographic and fractographic examination of fatigue loaded PM-steel with and without MnS additive. *Mater. Charact.* **2000**, *45*, 211–220. [CrossRef]

39. Enomoto, M. Nucleation of phase transformations at intragranular inclusions in steel. *Met. Mater.* **1998**, *4*, 115–123. [CrossRef]

40. Samsonov, G.V. *Physico-Chemical Properties of Oxides. Handbook*; Metallurgiya: Moscow, Russia, 1978; p. 130. (In Russian)

41. Brooksbank, D.; Andrews, K.W. Stress fields around inclusions and their relation to mechanical properties. *J. Iron Steel Inst.* **1972**, *210*, 246–255.

42. Touloukian, Y.S. *The Thermo-Physical Properties of High Temperatures of Solids Materials*; Macmillan Co.: New York, NY, USA, 1967; p. 462.

43. Sarma, D.S.; Karasev, A.V.; Jonsson, P.G. On the role of non-metallic inclusions in the nucleation of acicular ferrite in steels. *ISIJ Int.* **2009**, *49*, 1063–1074. [CrossRef]

44. Cverna, F. *Asm Ready Reference: Thermal Properties of Metals*; ASM International: Materials Park, OH, USA, 2002.

45. Pan, F.; Zhang, J.; Chen, H.L.; Su, Y.H.; Kou, C.L.; Su, Y.H.; Chen, S.H.; Lin, K.J.; Hsieh, P.H.; Hwang, W.S. Effects of rare earth metals on steel microstructures. *Materials* **2016**, *9*, 417. [CrossRef] [PubMed]